Check for updates

Bioscience Reports (2021) **41** BSR20210611
https://doi.org/10.1042/BSR20210611

PORTLAND PRESS

Research Article

SARS-CoV-2 spike protein S1 induces fibrin(ogen) resistant to fibrinolysis: implications for microclot formation in COVID-19

Lize M. Grobbelaar[1], Chantelle Venter[1], Mare Vlok[2], Malebogo Ngoepe[3,4], Gert Jacobus Laubscher[5], Petrus Johannes Lourens[5], Janami Steenkamp[1,6], Douglas B. Kell[1,7,8] and Etheresia Pretorius[1]

[1]Department of Physiological Sciences, Faculty of Science, Stellenbosch University, Stellenbosch, Private Bag X1, Matieland 7602, South Africa; [2]Central Analytical Facility: Mass Spectrometry Stellenbosch University, Tygerberg Campus, Room 6054, Clinical Building, Francie van Zijl Drive, Tygerberg, Cape Town 7505, South Africa; [3]Department of Mechanical Engineering, Faculty of Engineering and the Built Environment, University of Cape Town, Cape Town, Rondebosch 7701, South Africa; [4]Stellenbosch Institute for Advanced Study, Wallenberg Research Centre, Stellenbosch University, Stellenbosch, South Africa; [5]Private practice clinician, Mediclinic Stellenbosch, Stellenbosch 7600, South Africa; [6]PathCare Laboratories, PathCare Business Centre, PathCare Park, Neels Bothma Street, N1 City 7460, South Africa; [7]Department of Biochemistry and Systems Biology, Institute of Systems, Molecular and Integrative Biology, Faculty of Health and Life Sciences, University of Liverpool, Liverpool L69 7ZB, U.K.; [8]The Novo Nordisk Foundation Centre for Biosustainability, Technical University of Denmark, Kemitorvet 200, Kgs Lyngby 2800, Denmark

Correspondence: Etheresia Pretorius (resiap@sun.ac.za) or Douglas B. Kell (dbk@liv.ac.uk)

OPEN ACCESS

Severe acute respiratory syndrome coronavirus 2 (SARS-Cov-2)-induced infection, the cause of coronavirus disease 2019 (COVID-19), is characterized by unprecedented clinical pathologies. One of the most important pathologies, is hypercoagulation and microclots in the lungs of patients. Here we study the effect of isolated SARS-CoV-2 spike protein S1 subunit as potential inflammagen *sui generis*. Using scanning electron and fluorescence microscopy as well as mass spectrometry, we investigate the potential of this inflammagen to interact with platelets and fibrin(ogen) directly to cause blood hypercoagulation. Using platelet-poor plasma (PPP), we show that spike protein may interfere with blood flow. Mass spectrometry also showed that when spike protein S1 is added to healthy PPP, it results in structural changes to β and γ fibrin(ogen), complement 3, and prothrombin. These proteins were substantially resistant to trypsinization, in the presence of spike protein S1. Here we suggest that, in part, the presence of spike protein in circulation may contribute to the hypercoagulation in COVID-19 positive patients and may cause substantial impairment of fibrinolysis. Such lytic impairment may result in the persistent large microclots we have noted here and previously in plasma samples of COVID-19 patients. This observation may have important clinical relevance in the treatment of hypercoagulability in COVID-19 patients.

Introduction

Severe acute respiratory syndrome coronavirus 2 (SARS-Cov-2)-induced infection, the cause of coronavirus disease 2019 (COVID-19), is characterized by unprecedented clinical pathologies. Phenotypic vascular characteristics are strongly associated with various coagulopathies that may result in either bleeding and thrombocytopenia or hypercoagulation and thrombosis [1,2]. Various circulating and dysregulated inflammatory coagulation biomarkers, including fibrin(ogen), D-dimer, P-selectin and von Willebrand Factor (VWF), C-reactive protein (CRP), and various cytokines, directly bind to endothelial receptors. Endotheliopathies are therefore a key clinical feature of the condition [3,4]. During the progression of the various stages of the COVID-19, markers of viral replication, as well as VWF and fibrinogen depletion with increased D-dimer levels and dysregulated P-selectin levels, followed by a cytokine storm, are likely to be indicative of a poor prognosis [5–8]. This poor prognosis is further worsened as together with a

Received: 12 March 2021
Revised: 13 July 2021
Accepted: 29 July 2021

Accepted Manuscript Online: 30 July 2021
Version of Record published: 20 August 2021

© 2021 The Author(s). This is an open access article published by Portland Press Limited on behalf of the Biochemical Society and distributed under the Creative Commons Attribution License 4.0 (CC BY).

Downloaded from http://portlandpress.com/bioscirep/article-pdf/41/8/BSR20210611/919388/bsr-2021-0611.pdf by guest on 26 November 2022

Bioscience Reports (2021) **41** BSR20210611
https://doi.org/10.1042/BSR20210611

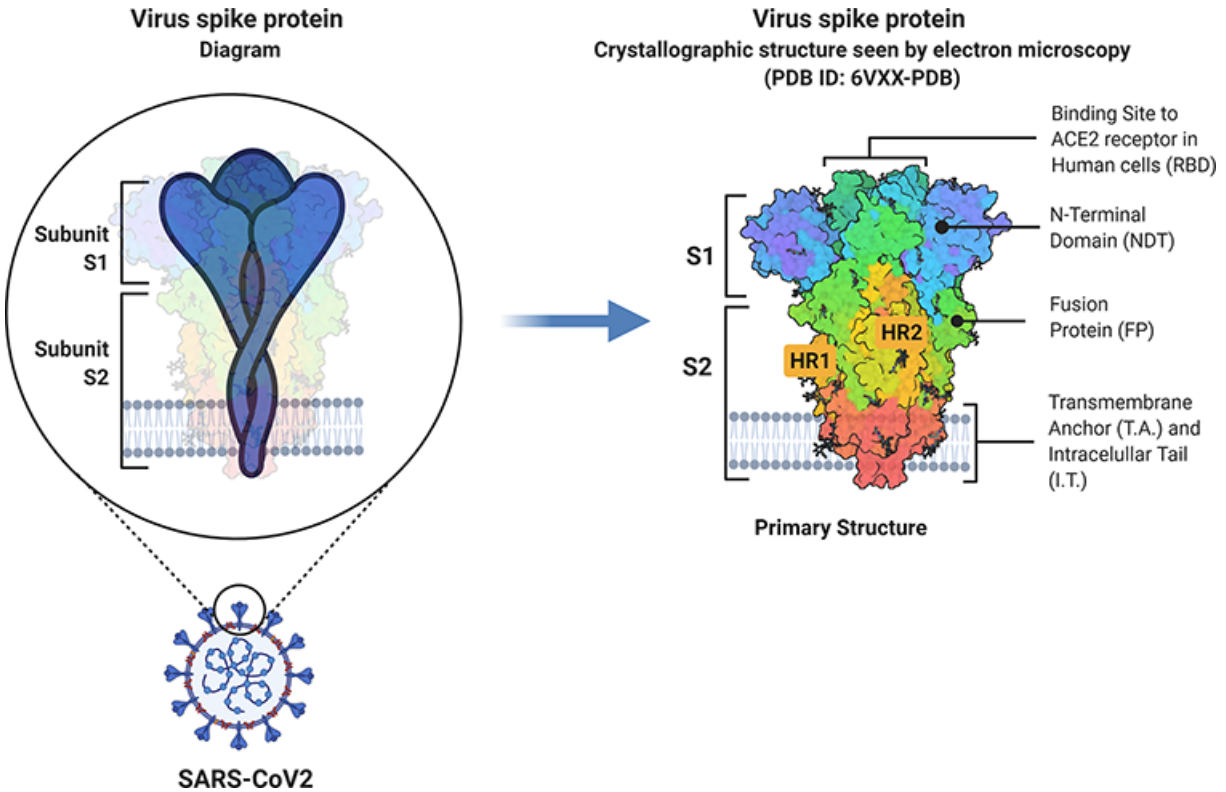

Figure 1. Schematic representation of SARS-CoV-2 Spike glycoprotein

Adapted from [21]. Abbreviations: HR1, heptad repeat 1; HR2, heptad repeat 2; S1, subunit 1; S2, subunit 2. This image was created with BioRender (https://biorender.com/).

substantial deposition of microclots in the lungs [9–11]. Plasma of COVID-19 patients also carries a massive load of preformed amyloid clots [5], and there are also numerous reports of damage to erythrocytes [12–14], platelets, and dysregulation of inflammatory biomarkers [5–8].

The virulence of the pathogen is closely linked to its membrane proteins. One such protein, found on the COVID-19 virus, is the spike protein, which is a membrane glycoprotein. The spike proteins are the key factors for virus attachment to target cells, as they bind to the angiotensin-converting 2 (ACE2) surface receptors [15]. Spike proteins are class I viral fusion proteins [16]. They are present as protruding homotrimers on the viral surface and mediate virus entry into the target host cells [17]. A singular spike protein is between 180 and 200 kDa in size and contains an extracellular N-terminal, a transmembrane domain fixed in the membrane of the virus, and a short intracellular C-terminal segment [16,18]. Spike proteins are coated with polysaccharide molecules that serve as camouflage. This helps evade surveillance by the host immune system during entry [18]. The S1 subunit is responsible for receptor binding [19], with subunit 2 (S2), a carboxyl-terminal subunit, responsible for viral fusion and entry [20] (see Figure 1).

Receptor binding is certainly responsible for cell-mediated pathologies, but does not itself explain the coagulopathies. Spike protein, can however be shed, and it has been detected in various organs, including the urinary tract [22]. S1 proteins can also cross the blood–brain barrier [23]. Free S1 particles may also play a role in the pathogenesis of the disease [24,25]. Free spike protein can potentially be released due to spontaneous 'firing' of the S protein trimers on the surface of virions, and infected cells liberates free receptor binding domain-containing S1 particles [24].

Here we study the effect of isolated SARS-CoV-2 spike protein S1 subunit as potential pro-inflammatory inflammagen *sui generis*. We investigate the potential of this inflammagen to directly interact with platelets and fibrin(ogen) to cause fibrin(ogen) protein changes and blood hypercoagulation. We also determine if the spike protein may interfere with blood flow, by comparing naïve healthy platelet-poor plasma (PPP) samples, with and without added spike protein, to PPP samples from COVID-19 positive patients (before treatment). We conclude that the spike protein may have pathological effects directly, without being taken up by cells. This provides further evidence that targeting it directly, whether via vaccines or antibodies, is likely to be of therapeutic benefit.

© 2021 The Author(s). This is an open access article published by Portland Press Limited on behalf of the Biochemical Society and distributed under the Creative Commons Attribution License 4.0 (CC BY).

Downloaded from http://portlandpress.com/bioscirep/article-pdf/41/8/BSR20210611/919388/bsr-2021-0611.pdf by guest on 26 November 2022

PORTLAND PRESS

Materials and methods

Sample demographics and considerations

Blood was collected from healthy volunteers (n=11; 3 males and 8 females; mean age: 43.4 $\pm$ 11.7 years) to serve as controls. Individuals who smoke, who were diagnosed with cardiovascular diseases, clotting disorders (coagulopathies), and/or any known inflammatory conditions (e.g. Type 2 Diabetes Mellitus (T2DM), rheumatoid arthritis, tuberculosis, asthma, etc.) could not serve as control volunteers. Furthermore, pregnancy, lactation, hormonal therapy, oral contraceptive usage, and/or using anticoagulants, were also factors that resulted in exclusion. Smoking was excluded since it has been proven to impair coagulation, fibrinolysis, and the hemostatic process [26]. Microfluidics analysis included a preliminary analysis using PPP samples from two COVID-19 positive patients, on the day of first diagnosis and before any treatment was given. Both patients were diagnosed with moderate to severe COVID-19 symptoms (1 male and 1 female, mean age: 78.5 $\pm$ 7.7 years).

Blood sample collection

Either a qualified phlebotomist or medical practitioner drew the volunteers' (control) blood via venepuncture, adhering to standard sterile protocol. Blood samples were stored in two to three 4.5-ml sodium citrate (3.2%) tubes (BD Vacutainer®, 369714). After several gentle inversions, the collected citrate tubes were allowed to rest at room temperature for a minimum of 30 min to allow for adequate anticoagulant amalgamation before commencing sample preparation. Whole blood (WB) was centrifuged at 3000×***g*** for 15 min at room temperature to isolate erythrocytes. The supernatant, i.e. PPP, was collected and stored in 1.5-ml Eppendorf tubes at −80°C, till needed for experiments.

Spike protein preparation

SARS-CoV-2 (2019-nCoV) Spike protein S1 Subunit, mFcTag, was purchased from Sino Biological (Beijing, China) (catalog number 40591-V05H1) and prepared using double distilled water, following the instructions provided. A total of 400 µl diluent (endotoxin-free water) was added to the 100 µg spike protein to create a stock solution (A) of 0.25 mg.ml^{-1}. This stock solution was diluted to working solutions. To determine the concentration of spike protein needed to result in significant, but yet a high enough concentration to cause physiological effects on the viscoelastic properties of blood, different concentrations of spike protein in PPP were assessed with fluorescence microscopy. A healthy control blood sample were separated into four 1.5-ml Eppendorf tubes with different final exposure concentrations of spike protein in the PPP of 100, 50, 10, and 1 ng.ml^{-1}. PPP samples were incubated with the various spike protein concentrations for 30 min at room temperature.

Fluorescence microscopy of purified fibrinogen and PPP with and without thrombin

Concentration verification

To verify which spike protein concentration will be effective, 5 µl of the PPP exposed to the varies spike protein concentrations was placed on a glass slide, after being exposed to the fluorescent amyloid dye, Thioflavin T (ThT) (Sigma–Aldrich, St. Louis, MO, U.S.A.) for 30 min at room temperature. The final concentration of ThT in all prepared samples was 0.005 mM. After the evaluation of the samples, with the varying spike protein concentrations, it was found that the final exposure concentration of 1 ng.ml^{-1} was sufficient and used for the rest of the study.

Amyloid protein and anomalous clotting in PPP samples

To study spontaneous anomalous clotting of fibrin(ogen), in the naïve healthy PPP samples, and in the presence of spike protein, 5 µl PPP exposed to 1 ng.ml^{-1} (final concentrations) of spike protein, was smeared on a glass slide and covered with a coverslip. This was done after it was exposed to the fluorescent amyloid dye, ThT (final concentration: 0.005 mM) (Sigma–Aldrich, St. Louis, MO, U.S.A.) for 30 min at room temperature. Fibrin PPP clots, with and without spike protein and after exposure to ThT, were also prepared by adding 2.5 µl of thrombin (7 U.ml^{-1}, South African National Blood Service) to 5 µl PPP and was placed on a glass slide and covered with a coverslip. The excitation wavelength for ThT was set at 450–488 nm and the emission at 499–529 nm and processed samples were viewed using a Zeiss Axio Observer 7 fluorescent microscope with a Plan-Apochromat 63×/1.4 Oil DIC M27 objective (Carl Zeiss Microscopy, Munich, Germany).

Fluorescence microscopy images of healthy PPP with and without spike protein were analyzed using Fiji® (Java 1.6_0 24 [64-bit]) to numerically represent the images. The total area of fluorescing particles or anomalous clotting (identified by the amyloid dye, ThT) [27–29] was determined using a thresholding algorithm in Fiji®. Images were firstly set to scale in Fiji® according to the magnification of the lens used on the fluorescent microscope, followed

Downloaded from http://portlandpress.com/bioscirep/article-pdf/41/8/BSR20210611/919388/bsr-2021-0611.pdf by guest on 26 November 2022

© 2021 The Author(s). This is an open access article published by Portland Press Limited on behalf of the Biochemical Society and distributed under the Creative Commons Attribution License 4.0 (CC BY).

Bioscience Reports (2021) **41** BSR20210611
https://doi.org/10.1042/BSR20210611

by the selection of appropriate threshold value to regard as much of the foreground and disregard as much of the background of the image as possible. In order to optimize the amount of images thresholded, a program was written in Java to simultaneously analyze a group of images (see Supplementary Material). The total percentage of anomalous clots in each image was calculated and the average of all the images per sample was calculated. These average values were used for statistical analysis.

Purified fibrin(ogen) clot model

To determine if spike protein causes changes in purified fibrinogen, our purified fibrin(ogen) clot model of choice was fluorescent fibrinogen conjugated to Alexa Fluor™ 488 (Thermo Fisher, F13191). A final fibrinogen concentration of 2 mg.ml^{-1} was prepared in endotoxin-free water and exposed to 1 ng.ml^{-1} (final concentrations) spike protein for 30 min at room temperature. A total of 5 μl of the purified fibrinogen was placed on a glass slide, with 2.5 μl of thrombin. The excitation wavelength for our fluorescent fibrinogen model was set at 450–488 nm and the emission at 499–529 nm and processed samples were viewed using a Zeiss Axio Observer 7 fluorescent microscope with a Plan-Apochromat 63×/1.4 Oil DIC M27 objective (Carl Zeiss Microscopy, Munich, Germany).

WB (hematocrit)

Hematocrit was exposed to a final exposure concentration of 1 ng.ml^{-1} spike protein. The fluorescent marker, CD62P (platelet surface P-selectin) was added to the hematocrit to study platelet activation. CD62P is found on the membrane of platelets and then translocated to the platelet membrane surface. The translocation occurs after the platelet P-selectin is released from the cellular granules during platelet activation [5,7]. A total of 4 μl CD62P (PE-conjugated) (IM1759U, Beckman Coulter, Brea, CA, U.S.A.) was added to 20 μl WB (either naïve or incubated with spike protein). The hematocrit exposed to the marker was incubated for 30 min (protected from light) at room temperature. The excitation wavelength for the CD62P was 540–570 nm and the emission 577–607 nm. Processed samples were also viewed using a Zeiss Axio Observer 7 fluorescent microscope with a Plan-Apochromat 63×/1.4 Oil DIC M27 objective (Carl Zeiss Microscopy, Munich, Germany).

Scanning electron microscopy of WB samples

Scanning electron microscopy (SEM) was used to view healthy WB samples, with and without the addition of spike protein. A total of 10 μl WB was placed on a glass coverslip and prepared according to previously published SEM preparation methods [30,31], starting with washing steps in phosphate-buffered saline (PBS) (pH = 7.4) (Thermo Fisher Scientific, 11594516) for 20 min. Fixation was performed by coating the slides in 4% formaldehyde (FA) for 30 min, followed by washing them in PBS three times. For each wash, the PBS should be left on for 3 min before removing and washing again. Osmium tetroxide (OsO_4) (Sigma–Aldrich, 75632) was added for 15 min and the slides were washed in PBS three-times with 3 min in each once more. The next step was to serially dehydrate the slides with ethanol followed by a drying step using hexamethyldisilazane (HMDS) (Sigma–Aldrich, 379212). Samples were mounted on glass slides and coated with carbon. The slides were viewed on a Zeiss MERLIN FE-SEM with the InLens detector at 1 kV (Carl Zeiss Microscopy, Munich, Germany).

Microfluidics

Microfluidic analysis was performed using healthy PPP and healthy pooled PPP samples (three pooled PPP samples), with and without spike protein, and two COVID-19 PPP samples. Pooled samples were used due to the volume required for this experiment.

Hardware

A microfluidic setup was used to simulate and investigate clot growth under conditions of flow. A Cellix microfluidic syringe pump (Cellix Ltd, Dublin, Ireland) was used to drive flow through Cellix Vena8 Fluoro+ biochips (Cellix Ltd, Dublin, Ireland), comprising eight straight microfluidic flow channels each, at flow rates specified in the following paragraph. A single microchannel had a width of 400 μm and a height of 100 μm (equivalent diameter of 207 μm), and a length of 2.8 cm. The dimensions of the microchannel were in the same order of magnitude as those of some vessels of the microvasculature, that is, under 300 μm [32]. In order to observe clot evolution in real-time, the biochips were placed under the Zeiss Axio Observer 7 fluorescent microscope with a 10×/0.25 objective (Carl Zeiss Microscopy, Munich, Germany).

Downloaded from http://portlandpress.com/bioscirep/article-pdf/41/8/BSR20210611/919388/bsr-2021-0611.pdf by guest on 26 November 2022

© 2021 The Author(s). This is an open access article published by Portland Press Limited on behalf of the Biochemical Society and distributed under the Creative Commons Attribution License 4.0 (CC BY).

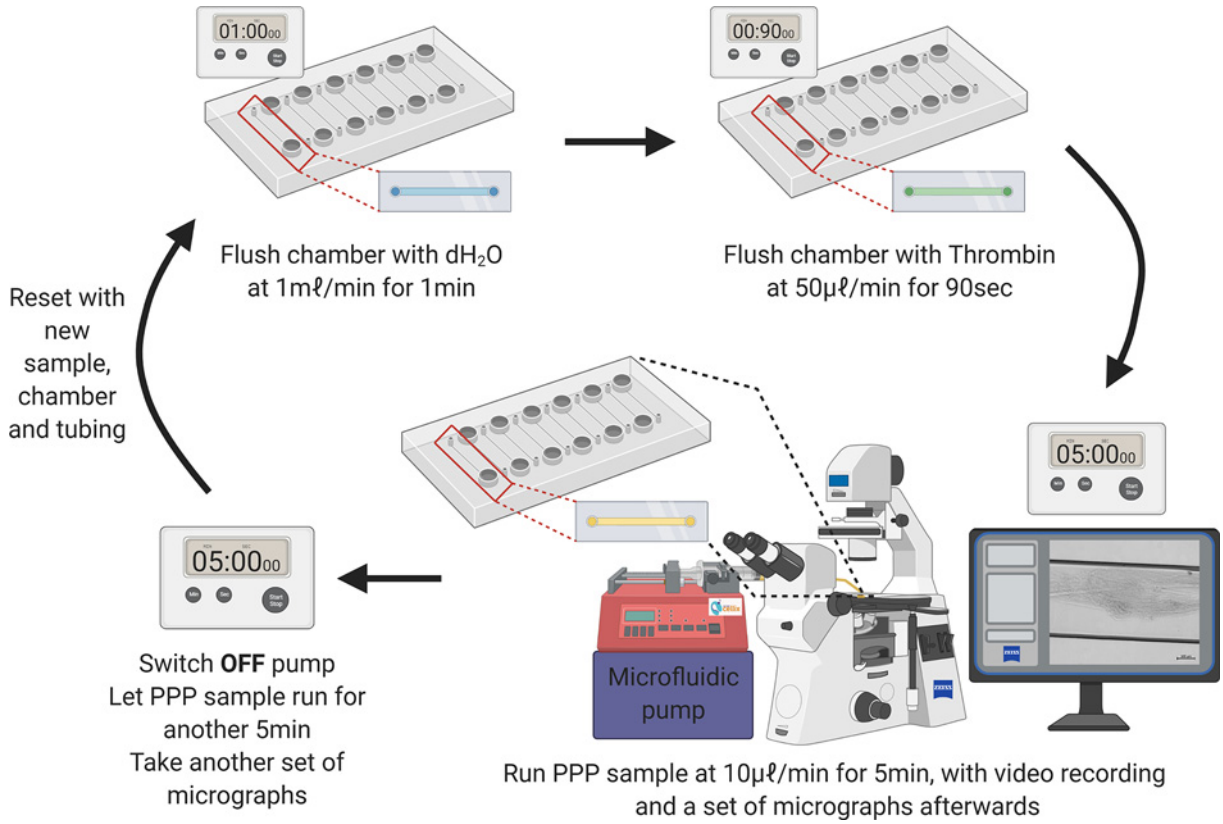

Figure 2. Experimental protocol for growing clots in a microfluidics system

Flow conditions

A new flow channel was used for every run. The channel was flushed with distilled water at a flow rate of 1 ml.min^{-1} for 1 min. After 5 min, thrombin was infused through the microchannel at a flow rate of 50 µl.min^{-1} for 90 s (Figure 2). The channel was left to stand for another 5 min and then the sample (control, control with spike, or COVID-19) was infused at a flow rate of 10 µl.min^{-1} for 5 min, with a video recording of the channel (Figure 2). The flow was then stopped after 5 min, and a set of micrographs was taken across the channel. The sample was then left for another 5 min, to see if any additional changes occur (Figure 2). This flow rate corresponds with a shear rate, $\gamma \approx 250\ s^{-1}$ and a Reynolds number, $Re \leq 1$. One of the main challenges in attempting to achieve consistent shear rates and Reynolds number was the variability in viscosity from sample to sample. Furthermore, blood flowing through microvessels is known to behave in a non-Newtonian manner, adding to the complexities of variable viscosity within a single sample. To achieve standardization between samples, a constant flow rate was used.

Proteomics

Four healthy PPP samples were analyzed before and after addition of spike protein. The samples were diluted in 10 mM ammonium bicarbonate to 1 mg.ml^{-1}. A total of 1 µg trypsin (New England Biosystems) was added to the plasma for 1:50 enzyme to substrate ratio. No reduction or alkylation was performed.

Liquid chromatography

Dionex nano-RSLC

Liquid chromatography was performed on a Thermo Scientific Ultimate 3000 RSLC equipped with a 5 mm × 300 µm C_{18} trap column (Thermo Scientific) and a CSH 25 cm × 75 µm, 1.7 µm particle size C_{18} column (Waters) analytical column. The solvent system employed was loading: 2% acetonitrile:water; 0.1% FA; Solvent A: 2% acetonitrile: water; 0.1% FA and Solvent B: 100% acetonitrile:water. The samples were loaded on to the trap column using loading solvent at a flow rate of 2 µl/min from a temperature controlled autosampler set at 7°C. Loading was performed for 5 min before the sample was eluted onto the analytical column. Flow rate was set to 300 nl/min and the gradient generated

© 2021 The Author(s). This is an open access article published by Portland Press Limited on behalf of the Biochemical Society and distributed under the Creative Commons Attribution License 4.0 (CC BY).

Downloaded from http://portlandpress.com/bioscirep/article-pdf/41/8/BSR20210611/919388/bsr-2021-0611.pdf by guest on 26 November 2022

Bioscience Reports (2021) **41** BSR20210611
https://doi.org/10.1042/BSR20210611

as follows: 5.0–30% B over 60 min and 30–50% B from 60–80 min. Chromatography was performed at 45°C and the outflow delivered to the mass spectrometer.

Mass spectrometry

Mass spectrometry was performed using a Thermo Scientific Fusion mass spectrometer equipped with a Nanospray Flex ionization source. Plasma samples, before and after addition of spike protein addition (1 $ng.ml^{-1}$ final exposure concentration), four of our control samples were analyzed with this method. The sample was introduced through a stainless-steel nano-bore emitter. Data were collected in positive mode with spray voltage set to 1.8 kV and ion transfer capillary set to 275°C. Spectra were internally calibrated using polysiloxane ions at $m/z = 445.12003$. MS1 scans were performed using the orbitrap detector set at 120000 resolution over the scan range 375–1500 with AGC target at 4 E5 and maximum injection time of 50 ms. Data were acquired in profile mode. MS2 acquisitions were performed using monoisotopic precursor selection for ion with charges +2 to +7 with error tolerance set to $\pm$10 ppm. Precursor ions were excluded from fragmentation once for a period of 60 s. Precursor ions were selected for fragmentation in HCD mode using the quadrupole mass analyzer with HCD energy set to 30%. Fragment ions were detected in the Orbitrap mass analyzer set to 30000 resolution. The AGC target was set to 5E4 and the maximum injection time to 100 ms. The data were acquired in centroid mode.

Statistical analysis

Data analysis: plasma samples

Statistical analyses of data generated were performed using GraphPad Prism software (version 9.0.0). The normality of the data was assessed using the Shapiro–Wilk normality test. For analysis of data between two groups, paired *t* tests (for pairwise statistical comparisons between data from untreated and treated control groups) and unpaired *t* tests (for non-pairwise statistical comparisons) were performed to assess statistical significance for parametric data, whereas the Mann–Whitney test was utilized to test for statistical significance in non-parametric data and the Wilcoxon's test was used for significance in paired parametric data. When comparing three or more experimental groups, the Kruskal–Wallis test (non-parametric data) or one-way ANOVA (parametric data) test was applied to test for statistical significance. A *P*-value of less than 0.05 was considered to be statistically significant. Parametric data were presented as the mean and standard deviation (SD), whereas non-parametric data were presented as the median and interquartile range (IQR).

Mass spectrometer data analysis

The raw files generated by the mass spectrometer were imported into Proteome Discoverer v1.4 (Thermo Scientific) and processed using the Sequest and Amanda algorithms. Database interrogation was performed against the 2019-nCOVpFASTA1 database. Semi-tryptic cleavage with two missed cleavages was allowed for. Precursor mass tolerance was set to 10 ppm and fragment mass tolerance set to 0.02 Da. Demamidation (NQ), oxidation (M) were allowed as dynamic modifications. Peptide validation was performed using the Target-Decoy PSM validator node. The search results were imported into Scaffold Q+ for further validation (www.proteomesoftware.com) and statistical testing. A *t* test was performed on the datasets and the emPAI quantitative method used to compare the datasets.

Supplementary material and raw data

All supplementary material and raw data can be accessed here: https://1drv.ms/u/s!AgoCOmY3bkKHisg5J0nb6wqsBzzWAQ?e=lmObMy

Results

Fluorescence microscopy of purified fibrinogen and PPP

Fluorescence microscopy was utilized to visualize the fluorescent amyloid signals in spontaneously formed anomalous clots, present in a fluorescent fibrinogen model, and also in healthy PPP with and without spike protein. As a preliminary investigation PPP from a single healthy control were incubated for 30 min with varying spike protein concentrations, followed by 30-min incubation with ThT and lastly preparation for viewing. It was found that the final exposure concentrations of 1 $ng.ml^{-1}$ was sufficient and used for the rest of the study (see supplementary raw data for other exposure concentrations' micrographs).

Figure 3A,B shows representative micrographs of purified fluorescent (Alexa Fluor™488) fibrinogen with added thrombin and after exposure to 1 $ng.ml^{-1}$ spike protein. A denser fibrin clot formed in the presence of spike protein (Figure 3B). In PPP, with and without thrombin, the green fluorescent ThT signal indicates areas of amyloid deposit

© 2021 The Author(s). This is an open access article published by Portland Press Limited on behalf of the Biochemical Society and distributed under the Creative Commons Attribution License 4.0 (CC BY).

Downloaded from http://portlandpress.com/bioscirep/article-pdf/41/8/BSR20210611/919388/bsr-2021-0611.pdf by guest on 26 November 2022

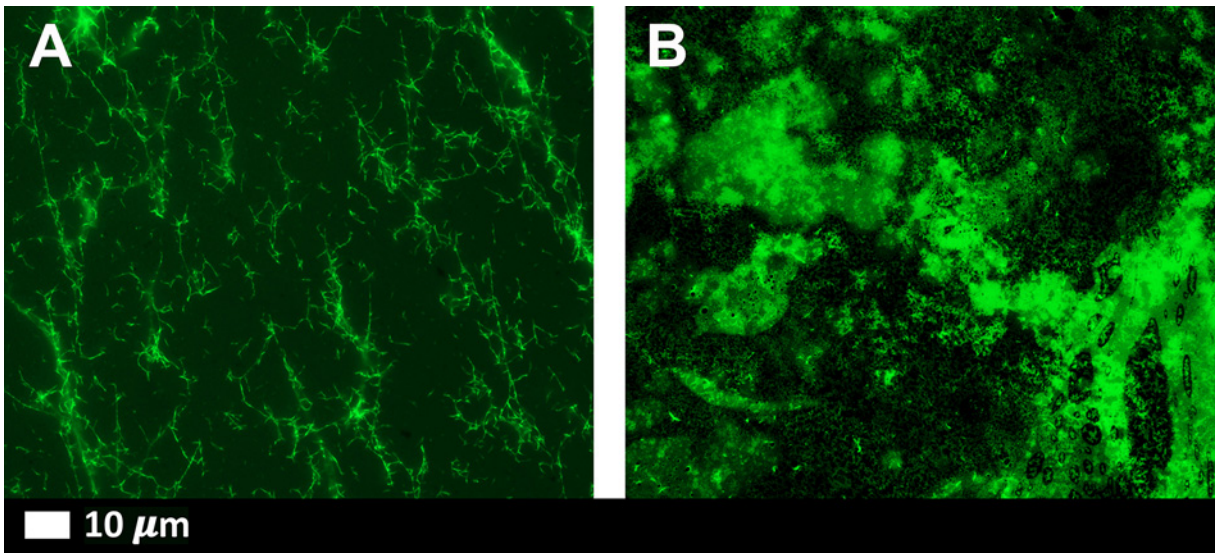

Figure 3. Representative fluorescence micrographs of purified fluorescent (Alexa Fluor™ 88) fibrinogen *(note no ThT added)* with added thrombin to form extensive fibrin clots

(**A**) Fluorescent fibrinogen with thrombin; (**B**) fluorescent fibrinogen with added spike protein (final exposure concentration 1 ng.ml^{-1}) and thrombin.

Table 1 Percentage average amyloid area in PPP with and without spike protein and with and without thrombin

Naïve healthy PPP vs naïve healthy PPP + added thrombin (*n*=10)	
P-value (Wilcoxon's test, paired non-parametric data expressed as median [Q1 − Q3]	0.2
Median of naïve healthy samples	0.3% [0.1–0.8%]
Median of naïve control samples (+ thrombin)	0.9% [0.3–1.5%]
Naïve healthy PPP + spike protein (1 ng.ml^{-1}) vs healthy PPP + spike protein (1 ng.ml^{-1}) + added thrombin) (*n*=10)	
P-value (data normally distributed; paired *t* test)	0.3
Mean percentage amyloid of healthy samples + spike	1.9% (±1.2%)
Mean percentage amyloid of healthy samples + spike (+ Thrombin)	2.4% (±1.3%)
Naïve healthy PPP vs healthy PPP + spike protein (1 ng.ml^{-1}) (*n*=10)	
P-value (Wilcoxon's test, paired non-parametric data expressed as median [Q1 − Q3]	**0.004 (*)**
Median of healthy samples	0.3% [0.1–0.8%]
Median of healthy samples + spike	1.9% [1.2–2.4%]
Naïve healthy PPP + added thrombin vs healthy PPP + spike protein (1 ng.ml^{-1}) + added thrombin) (*n*=10)	
P-value (data normally distributed; paired *t* test)	**0.0036 (*)**
Mean percentage amyloid of control samples (+ Thrombin)	0.9% (±0.6%)
Mean percentage amyloid of control samples + spike (+ Thrombin)	2.4% (1.3%)

Statistical significance was established at $P<0.05$. (* = $P<0.01$). Data are represented as either mean ± SD or median [Q1 − Q3].

formation. ThT is known to bind to open hydrophobic areas in protein and these are amyloid in nature [27,33–35]. Figure 4A,D shows representative micrographs of a healthy PPP smear, with and without thrombin, and with added ThT where slight anomalous clotting is seen. In contrast, when spike protein is added to PPP, with and without thrombin, a major increase in dense anomalous clotted deposits, with an amyloid nature, were noted (referred to as amyloid deposits) (Figure 4B,D). A thresholding algorithm was applied to the micrographs (with and without thrombin) using Fiji® which was used to calculate the total area of amyloid deposits in each micrograph (in total, 320 micrographs were analyzed). Using this method, the average total percentage of amyloid deposits per group was calculated (naïve healthy PPP, naïve healthy PPP + thrombin, and PPP incubated with 1 ng.ml^{-1} spike protein, with and without added thrombin) (see Table 1). As expected, there were no significant differences between % area amyloid deposits of healthy PPP with and without thrombin However, there was a significant increase in % area amyloid deposits in PPP before and after added spike protein, in both PPP smears and fibrin clots (where thrombin was added).

© 2021 The Author(s). This is an open access article published by Portland Press Limited on behalf of the Biochemical Society and distributed under the Creative Commons Attribution License 4.0 (CC BY).

Downloaded from http://portlandpress.com/bioscirep/article-pdf/41/8/BSR20210611/919388/bsr-2021-0611.pdf by guest on 26 November 2022

Bioscience Reports (2021) **41** BSR20210611
https://doi.org/10.1042/BSR20210611

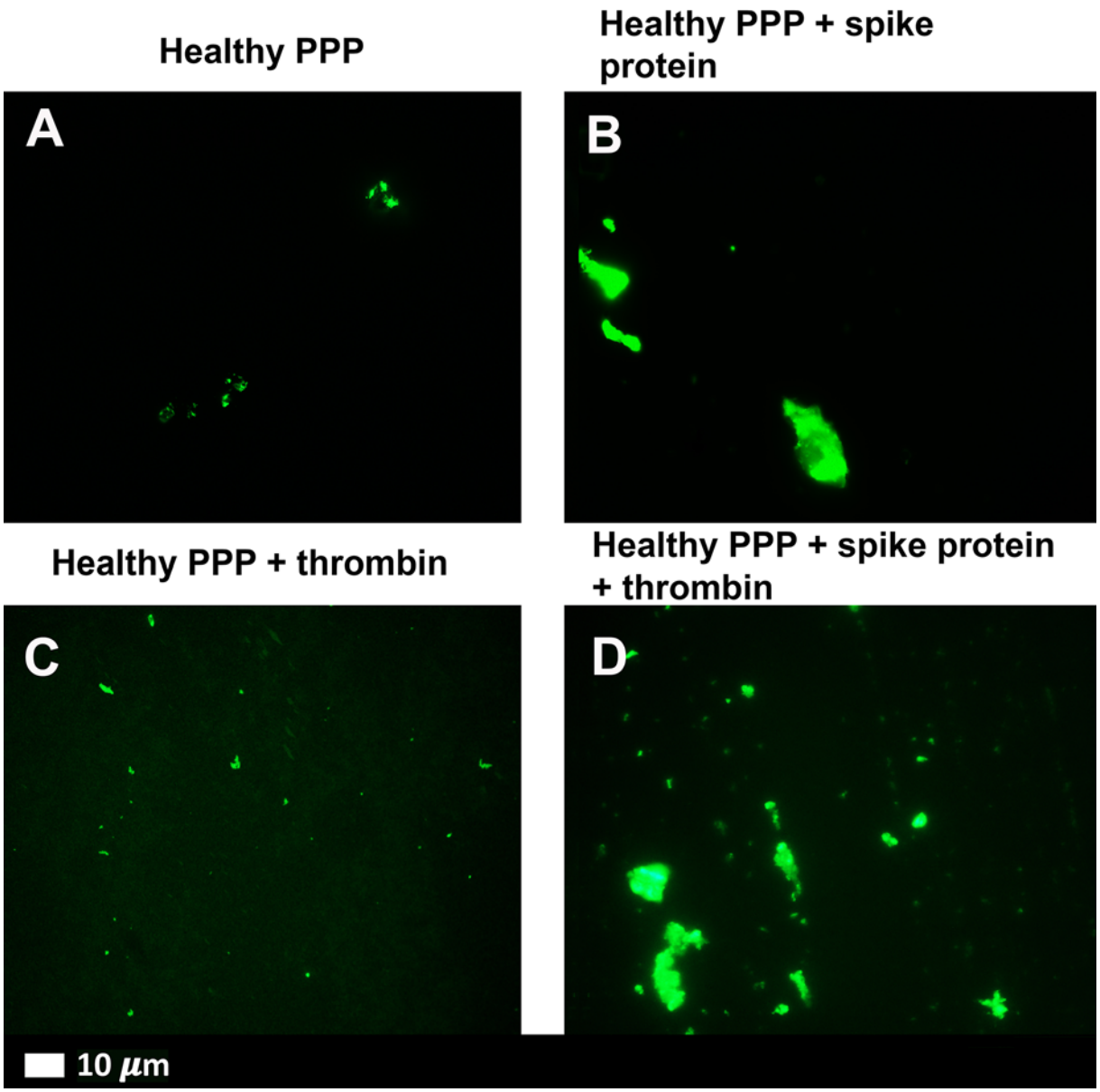

Figure 4. Representative fluorescence micrographs of PPP from healthy individuals after addition of ThT (green fluorescent signal)

(**A**) PPP smear. (**B**) PPP with spike protein. (**C**) PPP with thrombin to create extensive fibrin clot. (**D**) PPP exposed to spike protein followed by addition of thrombin. Final spike protein concentration was 1 ng.ml^{-1}.

Platelet activity

Fluorescence microscopy was used to visualize platelet activation in naive healthy hematocrit and hematocrit incubated with spike protein (1 ng.ml^{-1} final concentration). Samples were incubated with the platelet marker, CD62P-PE. Figure 5A shows representative platelets from naïve control samples, while Figure 5B shows micrographs after spike protein incubation. Spike protein caused an increase in platelet hyperactivation (Figure 5B arrows).

SEM of WB

SEM was used to assess the erythrocyte and platelet ultrastructure after treatment with spike protein (1 ng.ml^{-1} final concentration). Figure 6A,B shows micrographs from healthy WB samples, while Figure 6C–H shows micrographs of

© 2021 The Author(s). This is an open access article published by Portland Press Limited on behalf of the Biochemical Society and distributed under the Creative Commons Attribution License 4.0 (CC BY).

Downloaded from http://portlandpress.com/bioscirep/article-pdf/41/8/BSR20210611/919388/bsr-2021-0611.pdf by guest on 26 November 2022

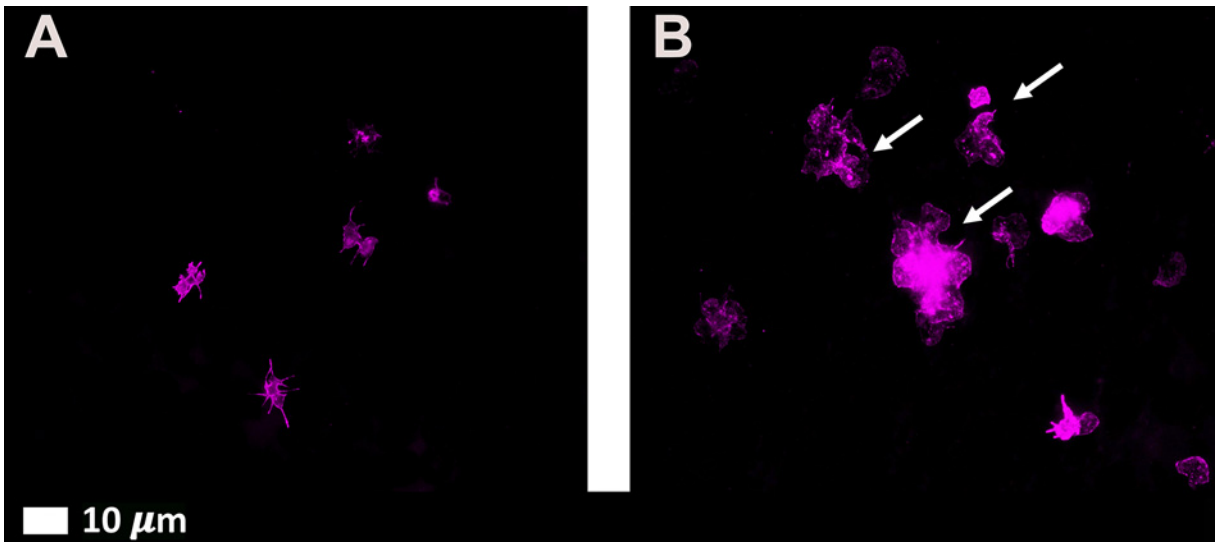

Figure 5. Fluorescence microscopy micrographs of platelets, before and after exposure to spike protein

(**A**) Representative platelets from hematocrit incubated with fluorescent marker, CD62P-PE. (**B**) Representative micrographs showing activated platelets after exposure to spike protein. The white arrows point to hyperactivated activated platelets. White arrows show hyperactivated platelets clumping together.

WB after incubation with spike protein. The majority of erythrocytes from healthy untreated controls were normocytic (regularly shaped) [Figure 6A (arrow)], and featured characteristic discoid shapes smooth, regular membrane surfaces. Slight platelet activation is seen due to contact activation (Figure 6B). The WB incubated with spike protein showed erythrocyte agglutination, despite the very low concentration of the spike protein. An increase in platelet hyperactivation, membrane spreading (Figure 6C,D), platelet-derived microparticle formation were noted due to spike protein exposure. The formation of spontaneous and anomalous fibrin(ogen) deposits with an amyloid nature, were prominent in all the samples incubated with spike protein, without the addition of thrombin [Figure 6E–H (arrows)].

Microfluidics

Figure 7 show the clots that formed in the flow chambers after 5 min of starting the experiment. Healthy PPP formed a small clot along the bottom surface of the channel, as seen in Figure 7A. In healthy plasma, clot formation was a relatively slow and gradual process, resulting in the formation of a modest clot (see Supplementary healthy PPP video S1). Clots formed in healthy PPP were relatively small and were limited to the walls of the flow channel. The clot had orderly layers that did not disrupt flow through the centre of the channel. As expected, clot formation was also less frequent than with the other samples (Figure 7B). The PPP with added spike protein showed a combination of a fibrous laminar clot and disorderly clotted mass (Figure 7E,F) (see Supplementary healthy PPP with added spike protein video S2). The COVID-19 PPP show disorderly clots that cover the bulk of the channel and often protruding into the center of the flow channel and disrupting flow (Figure 7C,D). In COVID-19 PPP, the reaction between thrombin and PPP occurred rapidly, resulting in large clots after approximately 90 s (see Supplementary pooled COVID-19 patient PPP video S3). Interestingly, these clots did not propagate much after the initial burst, indicating that most of the thrombin was consumed in a short period of time. Clots also formed with the PPP with the addition of the spike protein, but not as disruptive as the COVID-19 PPP clots.

An interesting observation was that clots from healthy PPP could easily be dislodged by flushing the flow channel with water at a rate of 1 $ml.min^{-1}$ (0.42 $m.s^{-1}$). Similarly, clots from healthy PPP with added spike protein could be dislodged in a similar fashion. COVID-19 clots, on the contrary, could not be displaced or dislodged and remained intact, even with the force of high-speed water flow in a small flow channel. This observation was consistent for all the COVID-19 samples.

Mass spectrometry analysis

Figure 8 shows results from the mass spectrometry analysis. Mass spectrometry showed that when spike protein is added to healthy PPP, it results in structural changes to β and γ fibrin(ogen), complement 3, and prothrombin.

© 2021 The Author(s). This is an open access article published by Portland Press Limited on behalf of the Biochemical Society and distributed under the Creative Commons Attribution License 4.0 (CC BY).

Downloaded from http://portlandpress.com/bioscirep/article-pdf/41/8/BSR20210611/919388/bsr-2021-0611.pdf by guest on 26 November 2022

Bioscience Reports (2021) **41** BSR20210611
https://doi.org/10.1042/BSR20210611

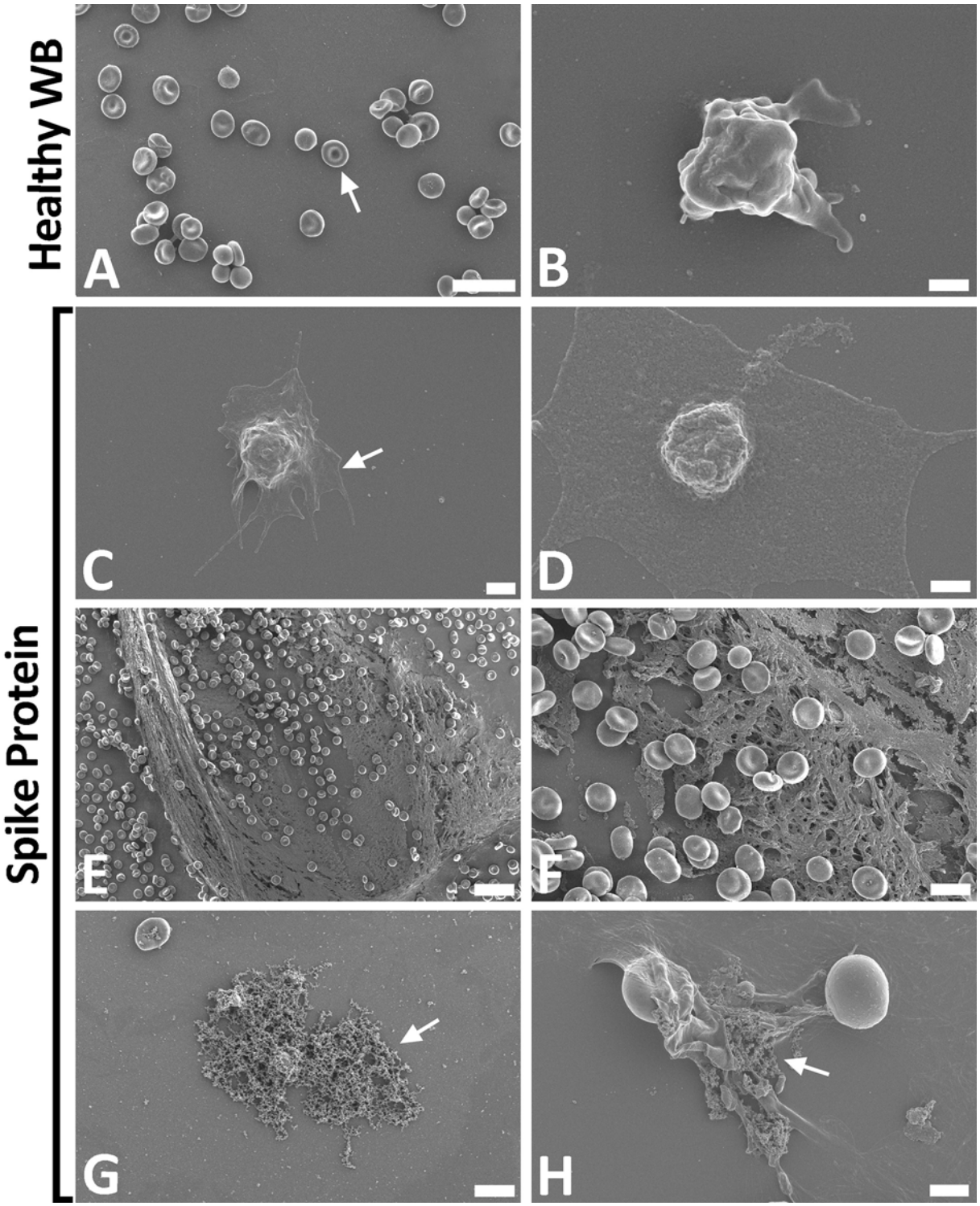

Figure 6. Whole blood sample of healthy volunteers, before and after exposure to spike protein

(**A–H**) Representative scanning electron micrographs of healthy control WB, with and without spike protein. (A,B) Healthy WB smears, with arrow indicating normal erythrocyte ultrastructure. (C–H) Healthy WB exposed to spike protein (1 ng.ml^{-1} final concentration), with (C,D) indicating the activated platelets (arrow), (E,F) showing the spontaneously formed fibrin network and (G,H) the anomalous deposits that is amyloid in nature (arrows) (scale bars: (E) 20 μm; (A) 10 μm; (F,G) 5 μm; (H) 2 μm; (C) 1 μm; (B,D) 500 nm).

Downloaded from http://portlandpress.com/bioscirep/article-pdf/41/8/BSR20210611/919388/bsr-2021-0611.pdf by guest on 26 November 2022

© 2021 The Author(s). This is an open access article published by Portland Press Limited on behalf of the Biochemical Society and distributed under the Creative Commons Attribution License 4.0 (CC BY).

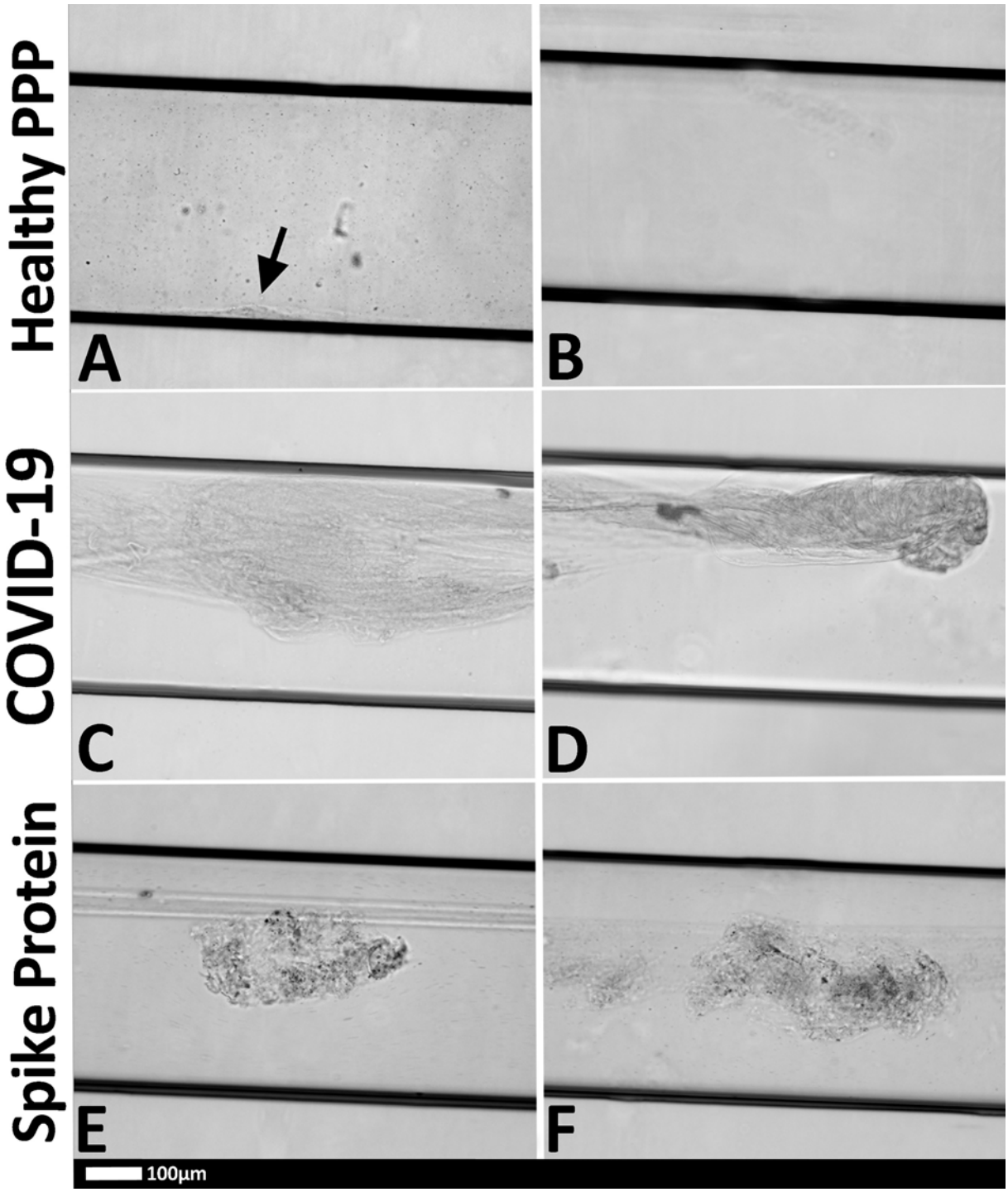

Figure 7. Representative micrographs of PPP clots in the microfluidic chambers (black horizontal lines are the outlines of the chambers) that were coated with thrombin

(**A**) Healthy PPP clot, with small clot formation (arrow), with (**B**) no clot formed in the healthy PPP sample. (**C,D**) examples of clots from COVID-19 PPP samples and (**E**,**F**) healthy PPP clot with spike protein. Black arrow = small clot formed in control sample; red arrows large clots in COVID-19 sample.

Downloaded from http://portlandpress.com/bioscirep/article-pdf/41/8/BSR20210611/919388/bsr-2021-0611.pdf by guest on 26 November 2022

© 2021 The Author(s). This is an open access article published by Portland Press Limited on behalf of the Biochemical Society and distributed under the Creative Commons Attribution License 4.0 (CC BY).

Bioscience Reports (2021) **41** BSR20210611
https://doi.org/10.1042/BSR20210611

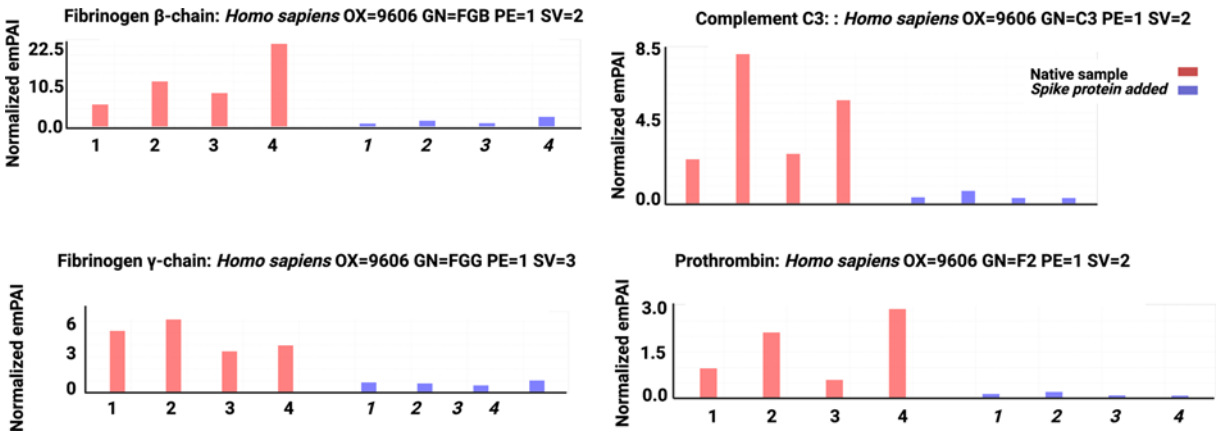

Figure 8. Mass spectrometry showing PPP of four samples with and without added spike protein

Spike protein results in structural changes to β and γ fibrin(ogen), complement 3, and prothrombin.

These proteins were substantially resistant to trypsinization, in the presence of spike protein (for sequence data, see supplementary files).

Discussion

In this laboratory analysis, we provide evidence that spike protein does indeed play a major role in hypercoagulability seen in COVID-19 patients. It causes anomalous clotting in both purified fluorescent fibrinogen and in PPP from healthy individuals, where the nature of the clots were shown to be amyloid (ThT as our amyloid dye of choice). An interesting observation was that these dense deposits were noted both in smears exposed to spike protein, and when thrombin was added. The addition of thrombin causes purified (Alexa Fluor™ 488) fibrinogen to polymerize into fibrin networks. Typically, these networks are net-like (Figure 3A). In the presence of spike protein, the structure changed to form dense clot deposits (Figure 3B). These deposits were seen in our fluorescent fibrin(ogen) model and PPP from healthy individuals exposed to spike protein. In healthy PPP exposed to spike protein, followed by incubation with ThT, there was a significant increase in anomalous clots with an amyloid nature, (Figure 4D), when compared with the healthy PPP. In the current paper, we did not analyze blood samples and clotting propensity of PPP from other patient cohorts, e.g. those with bacterial pneumonia or other acute viral diseases. However, our group (and others) have previously studied blood from HIV patients, where significant hypercoagulation in this patient cohort was noted [36–39]. We have also, recently, reported significant hypercoagulation in patients suffering from long COVID/PASC [40].

Spike protein also caused major ultrastructural changes in WB (as viewed with the SEM), where platelet hyperactivation was noted (Figure 6C,D). Increased in spontaneously formed fibrin network, as well as anomalous clot formation were also observed in SEM micrographs (Figure 6E–H). Interestingly, extensive spontaneous fibrin network formation was noted, without the addition of thrombin. This is in line with results that were recently published, where we showed similar ultrastructure in blood smears form COVID-19 positive patients. In these patients, platelet hyperactivation, anomalous clotting with amyloid signal, and spontaneous fibrin fiber formation were also observed [6,7].

With the microfluidics flow system, clots were formed, by infusing the entire microchannel with thrombin, thus simulating a hypercoagulable state, where endothelial damage was extensive. Given that the flow channel was made entirely of plastic and was devoid of any endothelial cells, the main component under investigation was the PPP (mostly fibrinogen protein) itself, which, in the case of the COVID-19 samples, may have contained downstream effects of some endothelial changes that would give rise to the hypercoagulable state that is characteristic of the disease. The flow setup used in the present study could not directly account for endothelial changes but nonetheless demonstrated that COVID-19 also results in changes in the clotting profile of the PPP. This was evident in the rapid rate of thrombin consumption and fibrin formation in COVID-19 clots, and also in the nature of the PPP clots that were formed.

The clots that were observed in the healthy PPP with added spike protein, were of particular interest as they demonstrated a bridge between healthy PPP clots and COVID-19 clots. As described in the 'Results' section, the healthy PPP clots were relatively small and orderly, while COVID-19 PPP clots were large, disorderly masses that formed rapidly

© 2021 The Author(s). This is an open access article published by Portland Press Limited on behalf of the Biochemical Society and distributed under the Creative Commons Attribution License 4.0 (CC BY).

Downloaded from http://portlandpress.com/bioscirep/article-pdf/41/8/BSR20210611/919388/bsr-2021-0611.pdf by guest on 26 November 2022

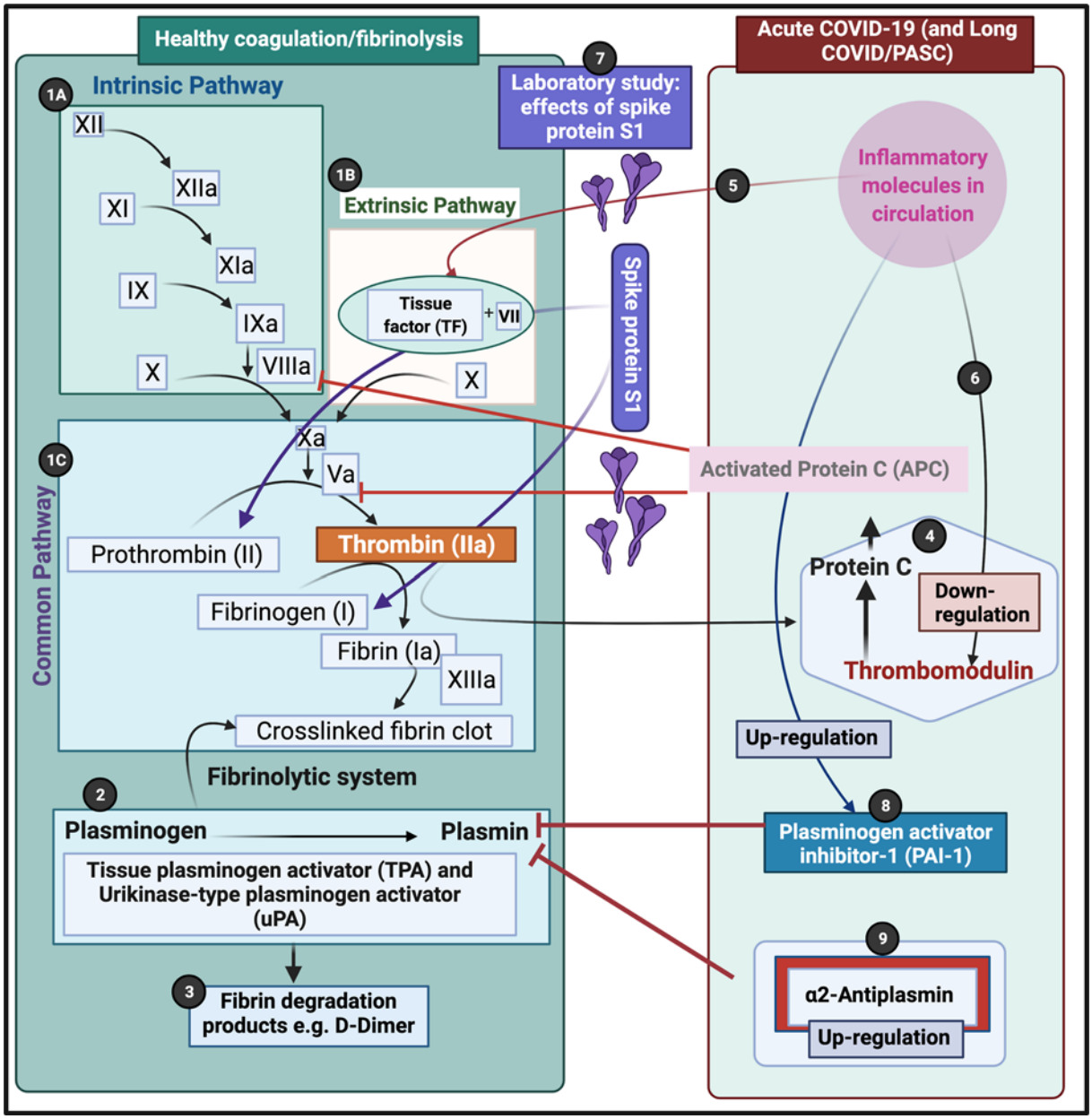

Figure 9. Simplified coagulation diagram depicting healthy and pathological processes

(**1A**) The intrinsic and (**1B**) extrinsic pathways converge into the (**1C**) common pathway. These pathways lead to the conversion of soluble fibrinogen to insoluble fibrin, catalyzed by thrombin. (**2**) Tissue plasminogen activator (tPA) or urokinase-type plasminogen activator (uPA) converts plasminogen into plasmin. A healthy fibrinolytic system regulates the coagulation pathway and assists with successful lysis of the insoluble fibrin clot. (**3**) Plasmin cleaves fibrin into fibrin degradation products (FDPs), including D-dimer. (**4**) Protein C and thrombomodulin both regulate coagulation: thrombin binds to its receptor, thrombomodulin, resulting in activated protein C (APC). APC then inhibits both Va and VIIIa. (**5**) Dysregulated inflammatory molecules may interfere with tissue factor (TF) expression. (**6**) Dysregulated inflammatory molecules may also down-regulate thrombomodulin, resulting in hypercoagulation, as Va and VIIIa activities are then not sufficiently modulated. (**7**) In our laboraoty suty, we added Spike protein S1 to healthy plasma. Pathophysiology was noted in both prothrombin and fibrinogen chains. (**8**) Dysregulated inflammatory molecules in circulation can inhibit of the fibrinolytic system via up-regulation of plasminogen activator inhibitor-1 (PAI-1). PAI-I up-regulation interferes with tPA function, and ultimately results in a dysregulated coagulation system. (**9**) α2AP inhibits plasmin and ultimately will prevent sufficient fibrinolysis to happen. (Figure created with Biorender.com).

Downloaded from http://portlandpress.com/bioscirep/article-pdf/41/8/BSR20210611/919388/bsr-2021-0611.pdf by guest on 26 November 2022

© 2021 The Author(s). This is an open access article published by Portland Press Limited on behalf of the Biochemical Society and distributed under the Creative Commons Attribution License 4.0 (CC BY).

Bioscience Reports (2021) **41** BSR20210611
https://doi.org/10.1042/BSR20210611

and disrupted PPP flow in the channel. The healthy PPP clots with added spike protein, were a combination of the two, demonstrating disorderly clumped clot areas, coexisting with laminar fibrous PPP clots (which were larger than the healthy PPP clots). This intermediate state may arise from a number of factors, including the interaction of other biological actors which were absent from the flow setup and the time of exposure to spike protein. Further investigations would be beneficial for understanding the clotting mechanisms that are altered in the presence of spike protein.

One of the obvious differences, which was inadvertently observed while trying to clean the channels with high-speed water flow (i.e. by mechanical means), was the ease of healthy PPP and healthy PPP with added spike protein clot dissolution. However, there was a complete failure to dislodge or disturb COVID-19 PPP clots from the channels. Given the clot lysis and dissolution is a complex interplay between biochemical and biophysical factors, investigation of the effects of different therapeutic agents could elucidate this phenomenon [41]. The flow protocol used in this study would be a useful platform for testing different treatments for clinical application. A further limitation of this exploration is the use of PPP in investigating clot formation at a scale appropriate to the microvasculature. While the protocol enables the study of fibrin microclots, which are of interest in COVID-19, it excludes the influence of RBCs, which are known to heavily influence the non-Newtonian flow behavior of blood at that scale [42]. The inaccuracy of the flow regime arising from this exclusion and from the variability of viscosity introduces error into the results. Nonetheless, the inclusion of flow an appropriate spatial scale has enabled us to observe COVID-19 PPP clot formation over space and time, under dynamic conditions, and has given insights which would otherwise prove difficult to glean.

A further avenue for exploration would include examining clot stability and removal for other patients with acute inflammatory responses arising from acute infections. Longstaff and co-workers found increased fibrinolytic resistance in inflammatory conditions arising from acute infection [43]. Examining this phenomenon in our microfluidic setup would be beneficial.

Given that microclots can block microcapillaries and thereby inhibit oxygen exchange, we have recently also studied plasma samples, using proteomics results from Long COVID/PASC, T2DM, with acute COVID-19 and compared results with plasma samples from healthy individuals. Interestingly, plasma from T2DM and form healthy individuals, immediately digested fully after a first trypsinization step, however, persistent microclots remained in the plasma samples from Long COVID/PASC and from acute COVID-19 samples, still contained large anomalous (amyloid) deposits (microclots) [40]. After a second trypsinization, the persistent pellet deposits were solubilized. We detected various inflammatory molecules that are substantially increased in both the supernatant and trapped in the solubilized pellet deposits of acute COVID-19 and Long COVID/PASC, versus the equivalent volume of fully digested fluid of the control samples and T2DM [40]. Of particular interest was a substantial increase in α(2)-antiplasmin (α2AP), various fibrinogen chains in both acute COVID-19 and Long COVID/PASC digested microclots. A comparison between healthy plasma and acute COVID-19 solubilized clots also showed a significant increase in coagulation factor XIII A chain, VWF Complement component C7 and CRP [40].

In the current study, mass spectrometry confirmed that spike protein causes structural changes to β and γ fibrin(ogen), complement 3, and prothrombin. These proteins become less resistant to trypsinization and changes the conformation, in such a way that there is a significant difference in peptide structure before and after spike protein addition. The current results therefore confirm results we have found in our recent proteomics analysis [40].

Our recent data suggest that there is an increase in (2)-antiplasmin inside the microclots of both acute COVID-19 and Long COVID, and we also note pathophysiology in the fibrinogen chains. In the present paper, we could induce fibrinogen chain pathology, after adding spike protein to healthy plasma. To result in an increase in molecules like α2-antiplasmin and VWF (and others), in patients with acute COVID-19 and also those with Long COVID/PASC, many physiological pathways should be activated. See Figure 9 (adjusted from [40, 44–46]) for a visual representation of the coagulation pathway and where it may be affected by S1.

Conclusion

Scanning electron- and fluorescence microscopy revealed large, dense anomalous and amyloid masses in WB and PPP of healthy individuals where spike protein was added to the samples. Mass spectrometry confirmed that when spike protein was added to PPP, it interacts with plasma proteins, resulting in fibrin(ogen), prothrombin and other proteins linked to coagulation, to become substantially resistant to trypsinization, resulting in less fragments. Flow analysis confirmed that microclots may impair blood flow. Here we suggest that, in part, the presence of spike protein S1 in circulation may contribute to the hypercoagulation in COVID-19 positive patients and may cause severe impairment of fibrinolysis. The effects of S2 might also be relevant, and should also be investigated in future. It is also now accepted that coagulation pathology is central in acute COVID-19 [47–52]. Several autopsy results have also

© 2021 The Author(s). This is an open access article published by Portland Press Limited on behalf of the Biochemical Society and distributed under the Creative Commons Attribution License 4.0 (CC BY).

Downloaded from http://portlandpress.com/bioscirep/article-pdf/41/8/BSR20210611/919388/bsr-2021-0611.pdf by guest on 26 November 2022

confirmed microthrombi throughout the lung and associated with right ventricular dilation of the heart. Recently, Ackermann and co-workers reported that histologic analysis of pulmonary vessels in patients with COVID-19 shows widespread thrombosis with microangiopathy [4]. The authors also showed that alveolar capillary microthrombi were nine-times as prevalent in patients with COVID-19 as in patients with influenza ($P<0.001$). Fibrinolytic impairment may therefore be the direct cause of the large microclots we have noted here in SEM and fluorescence microscopy, and previously in plasma samples of COVID-19 patients [6,7]. Clotting pathologies in acute COVID-19 infection might therefore benefit from following a regime of continued anticlotting therapy to support the fibrinolytic system function [40].

Data Availability

All supplementary material and raw data can be accessed here: https://1drv.ms/u/s!AgoCOmY3bkKHisg5J0nb6wqsBzzWAQ?e=XAsc7w

Competing Interests

The authors declare that there are no competing interests associated with the manuscript.

Funding

This work was supported by the Novo Nordisk Foundation [grant number NNF10CC1016517 (to Douglas B. Kell)].

Open Access

Open access for this article was enabled by the participation of University of Liverpool in an all-inclusive *Read & Publish* pilot with Portland Press and the Biochemical Society under a transformative agreement with JISC.

CRediT Author Contribution

Lize M. Grobbelaar: Formal analysis, Visualization, Writing—original draft. **Chantelle Venter:** Data curation, Project administration. **Mare Vlok:** Software, Formal analysis, Investigation. **Malebogo Ngoepe:** Methodology. **Gert Jacobus Laubscher:** Writing—review and editing. **Petrus Johannes Lourens:** Writing—review and editing. **Janami Steenkamp:** Project administration, Writing—review and editing. **Douglas B Kell:** Writing—review and editing. **Etheresia Pretorius:** Conceptualization, Resources, Formal analysis, Supervision, Funding acquisition, Validation, Investigation, Visualization, Methodology, Project administration, Writing—review and editing.

Ethics Approval

Ethical clearance for the study was obtained from the Health Research Ethics Committee (HREC) of Stellenbosch University (South Africa) (reference: N19/03/043, project ID: 9521). The experimental objectives, risks, and details were explained to volunteers both verbally and in text and informed consent were obtained prior to blood collection. Strict compliance to ethical guidelines and principles Declaration of Helsinki, South African Guidelines for Good Clinical Practice, and Medical Research Council Ethical Guidelines for Research were kept for the duration of the study and for all research protocols.

Consent for Publication

All authors approved submission of the paper.

Abbreviations

COVID-19, coronavirus disease 2019; CRP, C-reactive protein; FA, formaldehyde; PBS, phosphate-buffered saline; PPP, platelet-poor plasma; SARS-CoV-2, severe acute respiratory syndrome coronavirus 2; SEM, scanning electron microscopy; ThT, Thioflavin T; T2DM, Type 2 diabetes mellitus; VWF, von Willebrand Factor; WB, whole blood.

References

1 Gupta, A., Madhavan, M.V., Sehgal, K., Nair, N., Mahajan, S., Sehrawat, T.S. et al. (2020) Extrapulmonary manifestations of COVID-19. *Nat. Med.* **26**, 1017–1032, https://doi.org/10.1038/s41591-020-0968-3

2 Perico, L., Benigni, A., Casiraghi, F., Ng, L.F.P., Renia, L. and Remuzzi, G. (2021) Immunity, endothelial injury and complement-induced coagulopathy in COVID-19. *Nat. Rev. Nephrol.* **17**, 46–64, https://doi.org/10.1038/s41581-020-00357-4

3 Goshua, G., Pine, A.B., Meizlish, M.L., Chang, C.H., Zhang, H., Bahel, P. et al. (2020) Endotheliopathy in COVID-19-associated coagulopathy: evidence from a single-centre, cross-sectional study. *Lancet Haematol.* e575–e582, https://doi.org/10.1016/S2352-3026(20)30216-7

4 Ackermann, M., Verleden, S.E., Kuehnel, M., Haverich, A., Welte, T., Laenger, F. et al. (2020) Pulmonary vascular endothelialitis, thrombosis, and angiogenesis in Covid-19. *N. Engl. J. Med.* **383**, 120–128, https://doi.org/10.1056/NEJMoa2015432

© 2021 The Author(s). This is an open access article published by Portland Press Limited on behalf of the Biochemical Society and distributed under the Creative Commons Attribution License 4.0 (CC BY).

Downloaded from http://portlandpress.com/bioscirep/article-pdf/41/8/BSR20210611/919388/bsr-2021-0611.pdf by guest on 26 November 2022

5 Grobler, C., Maphumulo, S.C., Grobbelaar, L.M., Bredenkamp, J.C., Laubscher, G.J., Lourens, P.J. et al. (2020) Covid-19: The rollercoaster of fibrin(ogen), D-dimer, von Willebrand Factor, P-selectin and their interactions with endothelial cells, platelets and erythrocytes. *Int. J. Mol. Sci.* **21**, 5168, https://doi.org/10.3390/ijms21145168
6 Pretorius, E., Venter, C., Laubscher, G.J., Lourens, P.J., Steenkamp, J. and Kell, D.B. (2020) Prevalence of readily detected amyloid blood clots in 'unclotted' Type 2 diabetes mellitus and COVID-19 plasma: a preliminary report. *Cardiovasc. Diabetol.* **19**, 193, https://doi.org/10.1186/s12933-020-01165-7
7 Venter, C., Bezuidenhout, J.A., Laubscher, G.J., Lourens, P.J., Steenkamp, J., Kell, D.B. et al. (2020) Erythrocyte, platelet, serum ferritin, and P-selectin pathophysiology implicated in severe hypercoagulation and vascular complications in COVID-19. *Int. J. Mol. Sci.* **21**, 8234, https://doi.org/10.3390/ijms21218234
8 Roberts, I., Muelas, M.W., Taylor, J.M., Davison, A.S., Xu, Y., Grixti, J.M. et al. (2020) Untargeted metabolomics of COVID-19 patient serum reveals potential prognostic markers of both severity and outcome. *medRxiv*, https://doi.org/10.1101/2020.12.09.20246389
9 Renzi, S., Landoni, G., Zangrillo, A. and Ciceri, F. (2020) MicroCLOTS pathophysiology in COVID 19. *Korean J. Intern. Med.*, https://doi.org/10.3904/kjim.2020.336
10 Ciceri, F., Beretta, L., Scandroglio, A.M., Colombo, S., Landoni, G., Ruggeri, A. et al. (2020) Microvascular COVID-19 lung vessels obstructive thromboinflammatory syndrome (MicroCLOTS): an atypical acute respiratory distress syndrome working hypothesis. *Crit. Care Resusc.* **22**, 95–97
11 Bobrova, L., Kozlovskaya, N., Korotchaeva, Y., Bobkova, I., Kamyshova, E. and Moiseev, S. (2020) Microvascular COVID-19 lung vessels obstructive thromboinflammatory syndrome (MicroCLOTS): a new variant of thrombotic microangiopathy? *Crit. Care Resusc.* **22**, 284
12 Lam, L.M., Murphy, S.J., Kuri-Cervantes, L., Weisman, A.R., Ittner, C.A.G., Reilly, J.P. et al. (2020) Erythrocytes reveal complement activation in patients with COVID-19. *medRxiv*, https://doi.org/10.1101/2020.05.20.20104398
13 Berzuini, A., Bianco, C., Paccapelo, C., Bertolini, F., Gregato, G., Cattaneo, A. et al. (2020) Red cell-bound antibodies and transfusion requirements in hospitalized patients with COVID-19. *Blood* **136**, 766–768, https://doi.org/10.1182/blood.2020006695
14 Akhter, N., Ahmad, S., Alzahrani, F.A., Dar, S.A., Wahid, M., Haque, S. et al. (2020) Impact of COVID-19 on the cerebrovascular system and the prevention of RBC lysis. *Eur. Rev. Med. Pharmacol. Sci.* **24**, 10267–10278
15 Bergmann, C.C. and Silverman, R.H. (2020) COVID-19: coronavirus replication, pathogenesis, and therapeutic strategies. *Cleve. Clin. J. Med.* **87**, 321–327, https://doi.org/10.3949/ccjm.87a.20047
16 Kawase, M., Kataoka, M., Shirato, K. and Matsuyama, S. (2019) Biochemical analysis of coronavirus spike glycoprotein conformational intermediates during membrane fusion. *J. Virol.* **93**, e00785–19, https://doi.org/10.1128/JVI.00785-19
17 Walls, A.C., Park, Y.J., Tortorici, M.A., Wall, A., McGuire, A.T. and Veesler, D. (2020) Structure, function, and antigenicity of the SARS-CoV-2 spike glycoprotein. *Cell* **181**, 281.e286–292.e286, https://doi.org/10.1016/j.cell.2020.02.058
18 Zhang, C., Zheng, W., Huang, X., Bell, E.W., Zhou, X. and Zhang, Y. (2020) Protein structure and sequence re-analysis of 2019-nCoV genome does not indicate snakes as its intermediate host or the unique similarity between its spike protein insertions and HIV-1. *bioRxiv* **19**, 1351–1360, https://doi.org/10.1101/2020.02.04.933135
19 Watanabe, Y., Allen, J.D., Wrapp, D., McLellan, J.S. and Crispin, M. (2020) Site-specific glycan analysis of the SARS-CoV-2 spike. *Science* **369**, 330–333, https://doi.org/10.1126/science.abb9983
20 Flores-Alanis, A., Sandner-Miranda, L., Delgado, G., Cravioto, A. and Morales-Espinosa, R. (2020) The receptor binding domain of SARS-CoV-2 spike protein is the result of an ancestral recombination between the bat-CoV RaTG13 and the pangolin-CoV MP789. *BMC Res. Notes* **13**, 398, https://doi.org/10.1186/s13104-020-05242-8
21 Duan, L., Zheng, Q., Zhang, H., Niu, Y., Lou, Y. and Wang, H. (2020) The SARS-CoV-2 spike glycoprotein biosynthesis, structure, function, and antigenicity: implications for the design of spike-based vaccine immunogens. *Front. Immunol.* **11**, 576622, https://doi.org/10.3389/fimmu.2020.576622
22 George, S., Pal, A.C., Gagnon, J., Timalsina, S., Singh, P., Vydyam, P. et al. (2021) Evidence for SARS-CoV-2 spike protein in the urine of COVID-19 patients. *medRxiv*, https://doi.org/10.1101/2021.01.27.21250637
23 Rhea, E.M., Logsdon, A.F., Hansen, K.M., Williams, L.M., Reed, M.J., Baumann, K.K. et al. (2021) The S1 protein of SARS-CoV-2 crosses the blood–brain barrier in mice. *Nat. Neurosci.* **24**, 368–378, https://doi.org/10.1038/s41593-020-00771-8
24 Letarov, A.V., Babenko, V.V. and Kulikov, E.E. (2020) Free SARS-CoV-2 spike protein S1 particles may play a role in the pathogenesis of COVID-19 infection. *Biochemistry (Moscow)* **86**, 257–261, https://doi.org/10.1134/S0006297921030032
25 Buzhdygan, T.P., DeOre, B.J., Baldwin-Leclair, A., McGary, H., Razmpour, R., Galie, P.A. et al. (2020) The SARS-CoV-2 spike protein alters barrier function in 2D static and 3D microfluidic in vitro models of the human blood–brain barrier. *bioRxiv*
26 Pretorius, E., Oberholzer, H.M., van der Spuy, W.J. and Meiring, J.H. (2010) Smoking and coagulation: the sticky fibrin phenomenon. *Ultrastruct. Pathol.* **34**, 236–239, https://doi.org/10.3109/01913121003743716
27 Kell, D.B. and Pretorius, E. (2017) Proteins behaving badly. Substoichiometric molecular control and amplification of the initiation and nature of amyloid fibril formation: lessons from and for blood clotting. *Prog. Biophys. Mol. Biol.* **123**, 16–41, https://doi.org/10.1016/j.pbiomolbio.2016.08.006
28 Pretorius, E., Bester, J., Mbotwa, S., Robinson, C. and Kell, D.B. (2016) Acute induction of anomalous blood clotting by molecular amplification of highly substoichiometric levels of bacterial lipopolysaccharide. *J. R. Soc. Interface* **13**, 20160539, PMC5046953, https://doi.org/10.1098/rsif.2016.0539
29 Pretorius, E., Vermeulen, N., Bester, J., Lipinski, B. and Kell, D.B. (2013) A novel method for assessing the role of iron and its functional chelation in fibrin fibril formation: the use of scanning electron microscopy. *Toxicol. Mech. Methods* **23**, 352–359, https://doi.org/10.3109/15376516.2012.762082
30 Pretorius, E. (2013) The adaptability of red blood cells. *Cardiovasc. Diabetol.* **12**, 63, https://doi.org/10.1186/1475-2840-12-63
31 Pretorius, E., Vermeulen, N., Bester, J. and Lipinski, B. (2013) Novel use of scanning electron microscopy for detection of iron-induced morphological changes in human blood. *Microsc. Res. Tech.* **76**, 268–271, https://doi.org/10.1002/jemt.22163

Downloaded from http://portlandpress.com/bioscirep/article-pdf/41/8/BSR20210611/919388/bsr-2021-0611.pdf by guest on 26 November 2022

© 2021 The Author(s). This is an open access article published by Portland Press Limited on behalf of the Biochemical Society and distributed under the Creative Commons Attribution License 4.0 (CC BY).

32 Jacob, M., Chappell, D. and Becker, B.F. (2016) Regulation of blood flow and volume exchange across the microcirculation. *Crit. Care* **20**, 319, https://doi.org/10.1186/s13054-016-1485-0
33 Adams, B., Nunes, J.M., Page, M.J., Roberts, T., Carr, J., Nell, T.A. et al. (2019) Parkinson's disease: a systemic inflammatory disease accompanied by bacterial inflammagens. *Front. Aging Neurosci.* **11**, 210, https://doi.org/10.3389/fnagi.2019.00210
34 de Waal, G.M., Engelbrecht, L., Davis, T., de Villiers, W.J.S., Kell, D.B. and Pretorius, E. (2018) Correlative light-electron microscopy detects lipopolysaccharide and its association with fibrin fibres in Parkinson's disease, Alzheimer's disease and Type 2 diabetes mellitus. *Sci. Rep.* **8**, 16798, https://doi.org/10.1038/s41598-018-35009-y
35 Page, M.J., Thomson, G.J.A., Nunes, J.M., Engelbrecht, A.M., Nell, T.A., de Villiers, W.J.S. et al. (2019) Serum amyloid A binds to fibrin(ogen), promoting fibrin amyloid formation. *Sci. Rep.* **9**, 3102, https://doi.org/10.1038/s41598-019-39056-x
36 Jackson, B.S., Nunes Goncalves, J. and Pretorius, E. (2020) Comparison of pathological clotting using haematological, functional and morphological investigations in HIV-positive and HIV-negative patients with deep vein thrombosis. *Retrovirology* **17**, 14, https://doi.org/10.1186/s12977-020-00523-3
37 Jackson, B.S. and Pretorius, E. (2019) Pathological clotting and deep vein thrombosis in patients with HIV. *Semin. Thromb. Hemost.* **45**, 132–140, https://doi.org/10.1055/s-0038-1676374
38 Teer, E., Joseph, D.E., Driescher, N., Nell, T.A., Dominick, L., Midgley, N. et al. (2019) HIV and cardiovascular diseases risk: exploring the interplay between T-cell activation, coagulation, monocyte subsets, and lipid subclass alterations. *Am. J. Physiol. Heart Circ. Physiol.* **316**, H1146–H1157, https://doi.org/10.1152/ajpheart.00797.2018
39 Green, S.A., Smith, M., Hasley, R.B., Stephany, D., Harned, A., Nagashima, K. et al. (2015) Activated platelet-T-cell conjugates in peripheral blood of patients with HIV infection: coupling coagulation/inflammation and T cells. *AIDS* **29**, 1297–1308, https://doi.org/10.1097/QAD.0000000000000701
40 Pretorius, E., Vlok, M., Venter, C., Bezuidenhout, J.A., Laubscher, G.J., Steenkamp, J. et al. (2021) Persistent clotting protein pathology in Long COVID/post-acute sequelae of COVID-19 (PASC) is accompanied by increased levels of antiplasmin. *medRxiv*, https://doi.org/10.1101/2021.05.21.21257578
41 Hudson, N.E. (2017) Biophysical mechanisms mediating fibrin fiber lysis. *Biomed Res. Int.* **2017**, 2748340, https://doi.org/10.1155/2017/2748340
42 McHedlishvili, G. (1998) Disturbed blood flow structuring as critical factor of hemorheological disorders in microcirculation. *Clin. Hemorheol. Microcirc.* **19**, 315–325
43 Longstaff, C., Varjú, I., Sótonyi, P., Szabó, L., Krumrey, M., Hoell, A. et al. (2013) Mechanical stability and fibrinolytic resistance of clots containing fibrin, DNA, and histones. *J. Biol. Chem.* **288**, 6946–6956, https://doi.org/10.1074/jbc.M112.404301
44 Kell, D.B. and Pretorius, E. (2015) The simultaneous occurrence of both hypercoagulability and hypofibrinolysis in blood and serum during systemic inflammation, and the roles of iron and fibrin(ogen). *Integr. Biol. (Camb.)* **7**, 24–52, https://doi.org/10.1039/c4ib00173g
45 de Waal, G.M., de Villiers, W.J. and Pretorius, E. (2021) The link between bacterial inflammagens, leaky gut syndrome and colorectal cancer. *Curr. Med. Chem.*, https://doi.org/10.2174/0929867328666210219142737
46 Miszta, A., Huskens, D., Donkervoort, D., Roberts, M.J.M., Wolberg, A.S. and de Laat, B. (2021) Assessing plasmin generation in health and disease. *Int. J. Mol. Sci.* **22**, 2758, https://doi.org/10.3390/ijms22052758
47 Giannis, D., Ziogas, I.A. and Gianni, P. (2020) Coagulation disorders in coronavirus infected patients: COVID-19, SARS-CoV-1, MERS-CoV and lessons from the past. *J. Clin. Virol.* **127**, 104362, https://doi.org/10.1016/j.jcv.2020.104362
48 Kollias, A., Kyriakoulis, K.G., Dimakakos, E., Poulakou, G., Stergiou, G.S. and Syrigos, K. (2020) Thromboembolic risk and anticoagulant therapy in COVID-19 patients: emerging evidence and call for action. *Br. J. Haematol.* **189**, 846–847, https://doi.org/10.1111/bjh.16727
49 Middeldorp, S., Coppens, M., van Haaps, T.F., Foppen, M., Vlaar, A.P., Müller, M.C.A. et al. (2020) Incidence of venous thromboembolism in hospitalized patients with COVID-19. *J. Thromb. Haemost.* **18**, 1995–2002, https://doi.org/10.1111/jth.14888
50 Miesbach, W. and Makris, M. (2020) COVID-19: coagulopathy, risk of thrombosis, and the rationale for anticoagulation. *Clin. Appl. Thromb. Hemost.* **26**, 1076029620938149, https://doi.org/10.1177/1076029620938149
51 Levi, M., Thachil, J., Iba, T. and Levy, J.H. (2020) Coagulation abnormalities and thrombosis in patients with COVID-19. *Lancet Haematol.* **7**, e438–e440, https://doi.org/10.1016/S2352-3026(20)30145-9
52 Liu, P.P., Blet, A., Smyth, D. and Li, H. (2020) The science underlying COVID-19: implications for the cardiovascular system. *Circulation* **142**, 68–78, https://doi.org/10.1161/CIRCULATIONAHA.120.047549

Downloaded from http://portlandpress.com/bioscirep/article-pdf/41/8/BSR20210611/919388/bsr-2021-0611.pdf by guest on 26 November 2022

© 2021 The Author(s). This is an open access article published by Portland Press Limited on behalf of the Biochemical Society and distributed under the Creative Commons Attribution License 4.0 (CC BY).